

## **Micro-scale Investigation on Kinematic Behavior of Particulate Medium in Response to Shearing**

\*Quan Yuan<sup>1)</sup>, Pak-On Tam<sup>2)</sup>, Xia Li<sup>3)</sup>, Yu-Hsing Wang<sup>4)</sup>

<sup>1), 2), 4)</sup> *Department of Civil and Environmental Engineering, The Hong Kong University of Science and Technology, Hong Kong, P.R. China*

<sup>3)</sup> *Materials, Mechanics and Structures Research Division, Process and Environmental Division, Faculty of Engineering, University of Nottingham, UK*

<sup>4)</sup> [ceyhwang@ust.hk](mailto:ceyhwang@ust.hk)

### **ABSTRACT**

This paper reports the features of particle motion in response to shearing based on the experimental study using the Particle Image Velocimetry (PIV) technique. A tailor-made direct shear box equipped with an image system is used for this purpose. Wooden rods of three different diameters are randomly packed to form the sample. The particle displacements (at contacts) are decomposed into two parts, i.e., the rolling displacement and the sliding displacement and are obtained through the PIV analysis. Experimental results have demonstrated that particle rolling plays an important role in soil strength and dilatation. The peak and residual friction angles are greater than the interparticle friction angle due to an additional contribution from particle rolling. The particle rolling displacement becomes greater than the particle sliding displacement as the volumetric response transfers from contraction to dilation, suggesting particle rolling is a dominating mode of particle motion for soil dilation. Note that strong particle rotations are generated in particular areas and also continue to develop in the same area as the horizontal displacement increases.

### **1. INTRODUCTION**

It is widely reported the importance of particle rolling on influencing the behavior of particulate media based on both the experimental studies and numerical simulations that . (Matsuoka, 1974; Oda, 1982, 1998; Bardet and Proubet, 1992, 1994; Iwashita and

Oda, 1998, 2000; Yamamoto and Kunizawa, 2011; Zhao, 2011). Numerical simulation results have demonstrated that particle rolling has great influences on the shear strength. The peak and residual friction angles both are smaller than the interparticle friction angle if rolling resistance is not considered and particles are free to roll. Nevertheless, these two friction angles can be significantly increased after the rolling resistance model is introduced into the DEM simulations (Iwashita and Oda, 1998, 2000; Li, 2006; Lau and Wang, 2011).

Pure particle sliding in general is emphasized at the incipient stage of dilatancy whereas particle rolling is neglected (Newland and Allely, 1957; Rowe, 1962; Balendran and Nemat-Nasser, 1993); however, it has been illustrated by Dafalias (1994) that particle sliding induces contraction and rolling produces dilation. Oda and Kazama (1998) proposed a similar suggestion that rolling rather than sliding is the dominant mechanism governing dilatancy occurring in a shear band. From their point of view, buckling of columns and rolling at contacts take place as basic microdeformation mechanisms leading to dilatancy. Anandarajah (2004) presented a constitutive model for two-dimensional assembly of granular particles, based on a combination of interparticle sliding and rolling. Though most of salient features of the stress-strain behavior of granular materials can be satisfactorily simulated using his model, the experimental evidence have not been provided.

Nonetheless, the exact cause of soil dilation in response to shearing remains unclear at present. Hence, there is a strong need to carry out an experiment to explore the particle motions, including particle translation, rotation, rolling and sliding at contacts during shearing. The technique of particle image velocimetry (PIV), which is originally developed by White et al. (2003) for tracing the deformation of soil mass, is utilized herein to capture the motions of the two-dimensional rod particles.

## **2. EXPERIMENTAL DETAILS**

### *2.1 Modified direct shear apparatus*

Fig. 1 presents the experimental setup. A shear box was modified to have a transparent front side to facilitate tracing the motions of rods by the PIV technique. Two dial gages mounted vertically and horizontally were used to measure the vertical and horizontal displacement, respectively. A digital image system, i.e., a digital camera with a timer controller, was set to record the kinematics of particulate rods during shearing. A transparent sheet with reference dots was also mounted in front of the shear box for the PIV analyses.

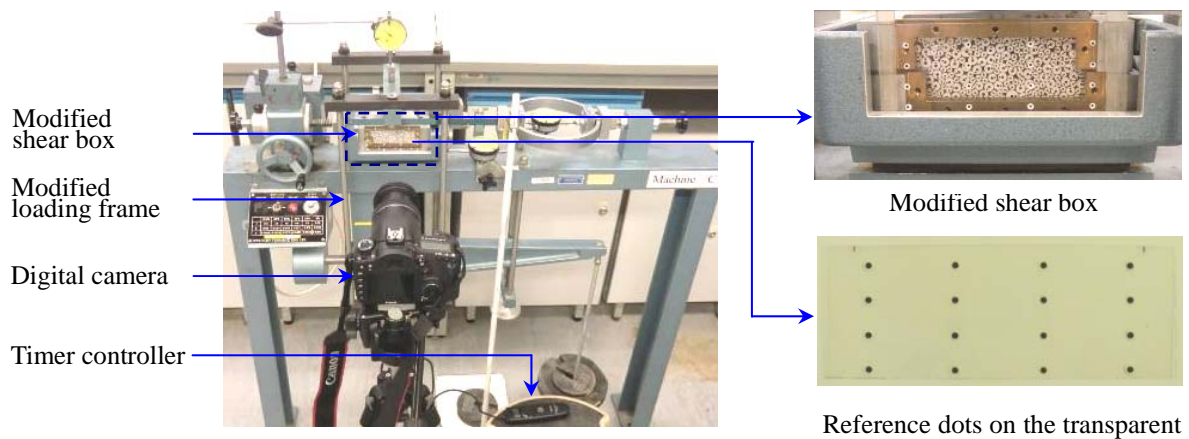


Fig.1 The experimental setup

## 2.2 Sample preparation and testing procedures

As shown in Fig. 2, commercially available wooden rods with three different sizes, 3.17 mm, 4.76 mm and 6.35 mm in diameter, were used to simulate sand particles. The rods length is 100 mm, which is corresponding to the inner dimension of the shear box. Two black dots were marked onto the white-painted rod ends, acting as references for tracing particle movement. One black dot was drawn at the center and the other one was drawn at the edge to form a direction vector associated with each rod. The rods were also numbered at the opposite ends of rods for identifications. The sample size was 45 mm in height and 100 mm in width. The sizes of wooden rods satisfied the requirement of ASTM D3080-90 that the ratios of the sample height and width to the maximum particle size have to be no less than 6 and 10, respectively. Rods of different sizes were assembled to form a random packing as shown in Fig. 1.

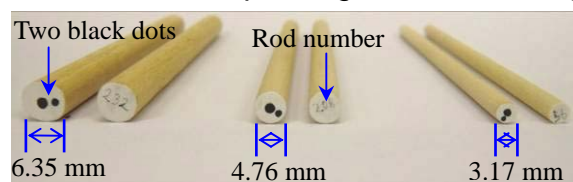


Fig. 2 Wooden rods used in the experiment

The experiment followed the normal procedure of direct shear box test. A vertical stress  $\sigma = 50$  kPa was applied in the experiment. The shear box was sheared with a speed of 0.1 mm/min and the image was taken automatically with a time interval of 1 minute. The corresponding vertical and horizontal displacements as well as the deformation of the proving ring were recorded manually every 1 minute.

## 2.3 Tracing particle motion

The principle and the procedure of the PIV have been demonstrated by White et al. (2003). The digital image (pixel) coordinates of the reference dots in the transparent

sheet were first obtained by advanced centroiding. Then, the relationship between the pixel coordinates and the real spatial coordinates can be established. Through this relationship, the pixel coordinates of the marked dots on the moving rods obtained by the PIV technique then can be converted into the real spatial coordinates, which were used to characterize the particle motion.

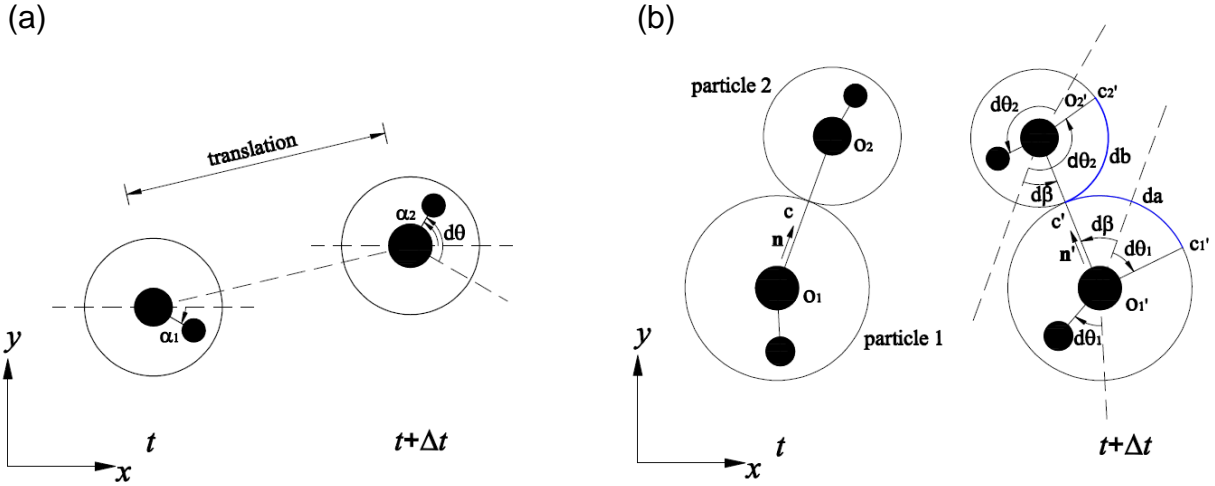


Fig. 3 Particle motions during time step from  $t$  to  $t+\Delta t$ . (a) particle translation and (b) particle rolling and sliding at contacts

As shown in Fig. 3a, both particle translation and rotation may happen simultaneously as the time is changed from  $t$  to  $t+\Delta t$ . The translation displacement can be calculated by the travel distance  $d\theta$  of the center of the marked dots before and after the particle movement. The angle of particle rotation  $d\theta$  is calculated by the rotation of the line that connects the marked dot in the center and the one at the edge.

Fig. 3b shows that two particles, i.e., particles 1 and 2, initially are in contact at point  $C$ , and then the contact is transferred to point  $C'$  after particle movement. The original contact point  $C$  is changed to be  $C_1'$  on particle 1 and  $C_2'$  on particle 2, respectively. The associated contact normals before and after particle movement are denoted by the vector  $\mathbf{n}$  and  $\mathbf{n}'$ . The associated rotating angle is noted as  $d\beta$ . The two particles are rotated by angles of  $d\theta_1$  and  $d\theta_2$  after moving to new positions (counterclockwise rotation is positive). The arc lengths of  $C'C_1'$  and  $C'C_2'$  as denoted by  $da$  and  $db$ , respectively, could be calculated by Eqs. (1) & (2):

$$da = r_1(d\theta_1 - d\beta), \quad (1)$$

$$db = r_2(d\theta_2 - d\beta) \quad (2)$$

Following the suggestion in Iwashita et al. (1998), these arc lengths associated with the contact point movement can be quantified by the rolling displacement  $dU_r$  and the sliding displacement  $dU_s$ , i.e.,

$$da = dU_r + dU_s \quad (3)$$

$$db = -dU_r + dU_s \quad (4)$$

Then, the amount of rolling and sliding displacements can be derived as Eqs. (5) & (6),

$$dU_r = \frac{da - db}{2} \quad (5)$$

$$dU_s = \frac{da + db}{2} \quad (6)$$

### 3 EXPERIMENTAL RESULTS & DISCUSSION

#### 3.1 Stress-strain and volumetric responses

Fig. 4a shows the stress-strain response in terms of the stress ratio  $\tau/\sigma$  versus the horizontal displacement  $\Delta x$  where  $\tau$  is the shear stress and  $\sigma$  is the vertical stress. Fig. 4b presents the volumetric response during shearing, in the manner of the vertical displacement  $\Delta z$  versus the horizontal displacement  $\Delta x$ . The sample contracts at the beginning of shearing and then shows a distinct dilation as  $\Delta x$  is about greater than 2 mm. The maximum dilatancy occurs at  $\Delta x$  is about 3.0 mm, which is very close to  $\Delta x$  at the peak stress, i.e., 3.2 mm.

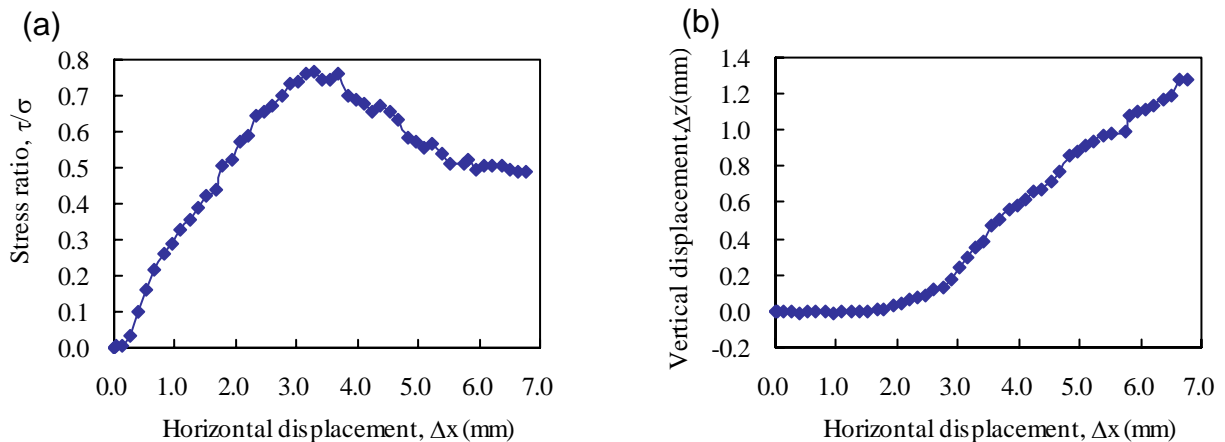


Fig. 4 Experimental results: (a) stress – strain and (b) volumetric responses

Fig. 5 presents the setup to measure the interparticle friction angle of rods. Two piles of rods with an applied loading of 10N were put on an inclined table, which is gradually elevated until the upper rod pile slides. The inclined angle of the table as rod pile slides is corresponding to the interparticle friction angle,  $24.82^\circ$ . As shown in Fig. 6, the mobilized peak and residual friction angles are  $37.4^\circ$  and  $26.3^\circ$ , respectively. Both the friction angles are greater than the interparticle friction angle, suggesting additional contributions from particle rolling and rearrangement to the macroscopic friction angles.

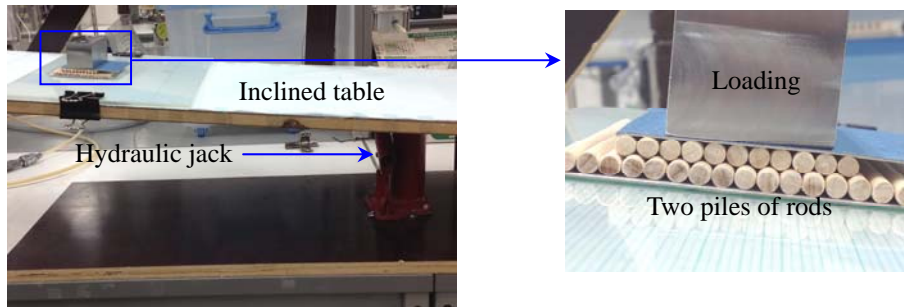


Fig. 5 Experimental setup to measure the interparticle friction angle of the wooden rods

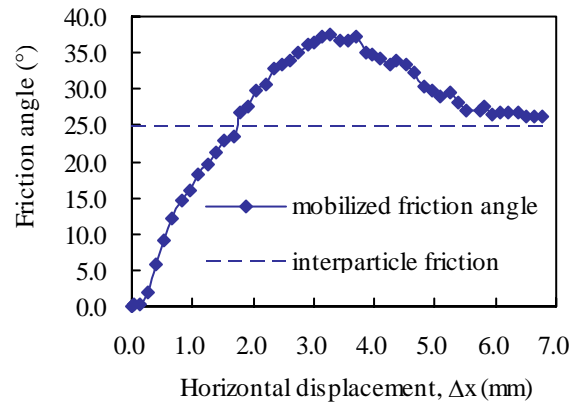


Fig. 6 Interparticle friction angle and mobilized friction angles in response to shearing

### 3.2 Particle displacement

Fig. 7 presents the displacement vectors of traced particles at  $\Delta x = 1.09$  mm, 3.28 mm and 5.24 mm. A dotted line is added in the figure to indicate the boundary between the upper and bottom boxes. The magnitudes of the vectors are scaled up by 10 times of their real value for clearer presentations. The tendency of the particle translation inclines to the right direction due to the sample sheared towards right. The magnitudes of the vectors in the lower box, which is the moving box during shearing, exhibit larger values than those observed for particles inside the upper box. The particle displacements generate a field of relative uniform at the beginning with  $\Delta x = 1.09$  mm. These displacement vectors also gradually move towards the right upper direction at  $\Delta x = 3.28$  mm, and this phenomenon becomes more obvious  $\Delta x = 5.24$  mm. This response might be explained using the DEM simulation result in Zhang and Thornton (2007) that the force transmission in the sample concentrates in the diagonal zone. This in turns leads particles to move in the same direction.

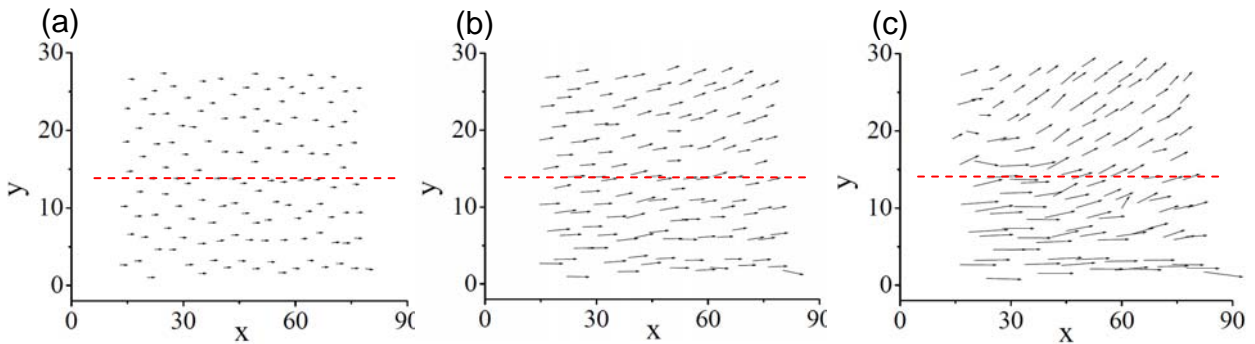


Fig. 7 Displacement vector at (a)  $\Delta x = 1.09$  mm;  $\Delta x = 3.28$  mm; and (c)  $\Delta x = 5.24$  mm

### 3.3 Particle rotation

Fig. 8 presents contours of particle rotations also corresponding to horizontal displacements  $\Delta x = 1.09$  mm, 3.28mm and 5.24mm. The particle rotation is presented by the rotation angle with a positive sign denoting the counterclockwise direction. The boundary between the upper and bottom boxes are indicated by a dotted line in the figure again. It appears that most of the particles are only slightly rotated in response to shearing, as presented by the green or pale green regions. The particle rotations are randomly distributed when the horizontal displacement is still small, i.e., for the case at  $\Delta x = 1.09$  mm. Then, strong particle rotations are generated in particular areas and also continue to develop in the same area as  $\Delta x$  is increased to 3.28 mm and 5.24 mm. These experimental observations imply the findings of DEM simulation reported in Bardet (1994): the particle rotation has significant effects on the shear strength. Note that some of the applied energy has been used to make particle rotate.

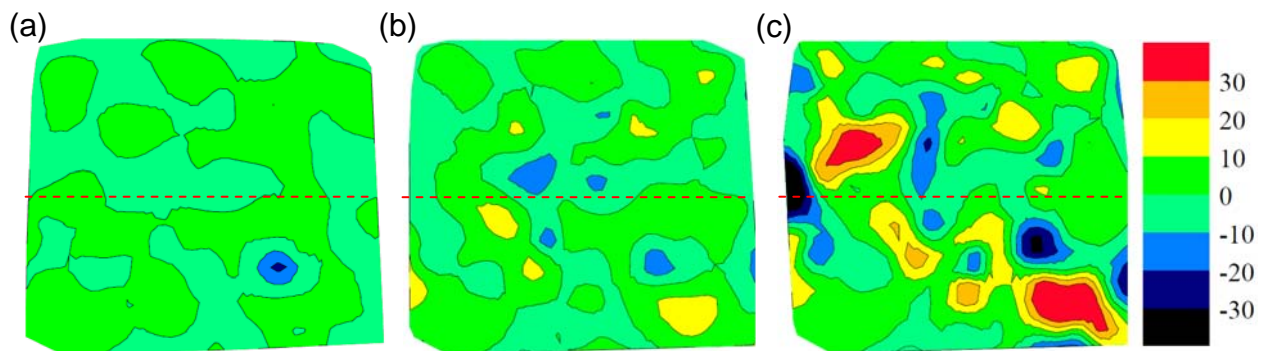


Fig. 8 Rotation contour at (a)  $\Delta x = 1.09$  mm;  $\Delta x = 3.28$  mm; and (c)  $\Delta x = 5.24$  mm

### 3.4 Rolling and sliding displacements at contacts

The rolling displacement  $dU_r$  and sliding displacement  $dU_s$  quantified by Eqs. (5) & (6) are used to continue exploring the importance of particle rolling in developing soil strength and dilatancy. Fig. 9 shows the corresponding rolling and sliding displacements at different shear displacements. Each data point represents the average value of rolling or sliding displacements of those contacts whose displacements regardless of rolling or

sliding are greater than the associated mean calculated from the displacements of all contacts. The dotted line in the figure indicates the horizontal displacement is equal to 2 mm where the sample begins to show a strong dilation response. It can be seen that the rolling displacement gradually becomes greater than the sliding displacement after  $\Delta x$  is greater than 2 mm. Such a trend behavior is more distinct as  $\Delta x$  increases. This echoes the suggestion in Dafalias (1994) that particle sliding produces volumetric contraction to make denser packing; nevertheless, particle rolling leads to dilatational volumetric strains by causing some particles to roll over neighboring particles.

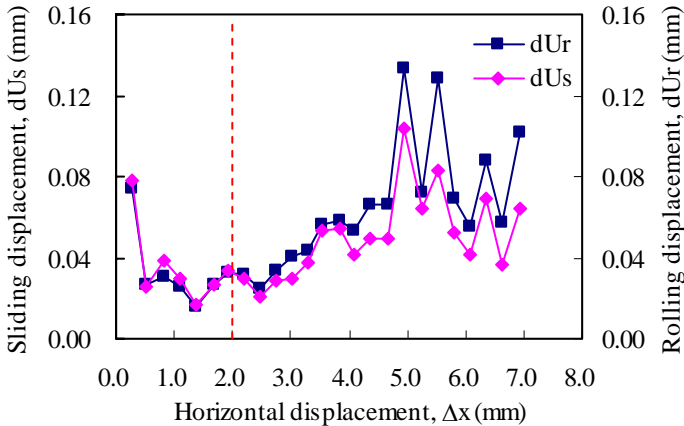


Fig. 9 Rolling and sliding displacement in response to shearing

Fig. 10 presents the correlation between the rolling displacement and the sliding displacement. The correlation appears to be positive with  $R^2$  value of 0.81, denoting that both the particle rolling and sliding occur simultaneously during shearing. It also shows that the best fit line inclines to the rolling displacement axis, especially for large displacements. This, once again, suggests that the rolling displacement gradually dominates the particle motion and overwhelms the opposite effect, i.e., the sliding displacement, and ultimately gives rise to soil dilation.

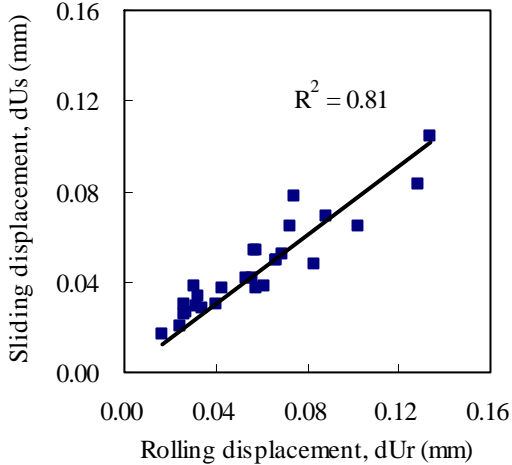


Fig. 10 Correlation between rolling and sliding displacement in response to shearing

#### 4. CONCLUSIONS

In this study, the PIV technique was adopted to characterize the particle movement in response to shearing. It has been found that particle rolling can affect the soil strength and associated friction angles. This can be reflected in that experimental result that the peak and residual friction angles are greater than the interparticle friction angle. The particle rotations are randomly distributed when the horizontal displacement  $\Delta x$  is still small. Then strong particle rotations are generated in particular areas and also continue to develop in the same area as  $\Delta x$  increases. The rolling displacement gradually dominates the particle motion and overwhelms the sliding displacement as  $\Delta x$  increases; this ultimately gives rise to soil dilation.

#### Acknowledgements

This research was supported by the Hong Kong Research Grants Council (GRF 620310).

#### REFERENCES

- Anandarajah, A. (2003), "Sliding and rolling constitutive theory for granular materials," *Journal of Engineering Mechanics*, 130(6), 665-680.
- White, D. J. Take, W. A. and Bolton, M. D. (2003), "Soil deformation measurement using particle image velocimetry (PIV) and photogrammetry," *Geotechnique Géotechnique*, 7, 619-631.
- Balendran, B. and Nemat-Nasser, S. (1993), "Double sliding model for cyclic deformation of granular materials, including dilatancy effects," *Journal of the Mechanics and Physics of Solids*, 41(3), 573-612.
- Bardet, J. P. (1994), "Observations on the effects of particle rotations on the failure of idealized granular materials," *Mechanics of Materials*, 18, 159-182.
- Bardet, J. P. and Proubet, J. (1992), "A shear band analysis in idealized granular materials," *Journal of Engineering Mechanics*, ASCE 118(2), 397-415.
- Bardet, J. P. and Proubet, J. (1992), "An numerical investigation of the structure of persistent shear bands in granular media," *Geotechnique*, 41(4), 599-613.
- Dafalias, Y. F. (1993), "Overview of constitutive models used in VELACS," *Proceedings of the International Conference on the Verification of Numerical Procedures for the Analysis of Soil Liquefaction Problems*, California, 1293-1303.
- Iwashita, K. and Oda, M. (1998), "Rolling resistance at contacts in simulation of shear band development by DEM," *Journal of Engineering Mechanics*, 124(3), 285-292.
- Lau, Y. M. and Wang, Y. H. (submitted, 2011), "DEM simulations on triaxial tests Discrete element method simulations of triaxial tests and triaxial creep tests," Mphil thesis, The Hong Kong University of Science and Technology. *Journal of Geotechnical and Geoenvironmental Engineering*.

- Li, X. (2006), "Micro-scale investigation on the quasi-static behavior of granular material," Ph.D thesis, The Hong Kong University of Science and Technology, 299-309.
- Matsuoka, H. (1974), "A microscopic study on shear mechanism of granular materials," *Soils and Foundations*, 14(1), 29-43.
- Newland, P. L. and Allely, B. H. (1957), "Volume changes in drained triaxial tests on granular materials," *Geotechnique Géotechnique*, 7, 17-34.
- Rowe, P. W. (1962), "The stress-dilatancy relation for static equilibrium of an assembly of particles in contact," *Proceedings of the Royal Society, London*, 500-527.
- Oda, M. and Iwashita, K. (2000), "Study on couple stress and shear band development in granular media based on numerical simulation analyses," *International Journal of Engineering Science*, 38, 1713-1740.
- Oda, M. and Kazama, H. (1998), "Microstructure of shear bands and its relation to the mechanisms of dilatancy and failure of dense granular soils," *Geotechnique Géotechnique*, 48(4), 465-481.
- Oda, M., Konishi, J. and Nemat-Nasser, S. (1982), "Experimental micromechanical evaluation of strength of granular materials: effects of particle rolling," *Mechanics of Materials*. 1, 262-283.
- Yamamoto, H. and Kunizawa, H. (2011), "Displacement and rotation measurements of particles in shear zone," *Proceedings of the Fifth International Symposium on Deformation Characteristics of Geomaterials*, IS Seoul, 513-519.
- Zhang, L. and Thornton. C. (2007), "A numerical examination of the direct shear test," *Géotechnique Geotechnique*, 57(4), 343-354.
- Zhao, X. L. (2011), "Numerical modeling of granular assembly using discrete element method," *Advanced Materials Research Vols. 146-147*, 738-742.